Electrocatalytic conversion of G-type and S-type phenolic compounds from different tree species in a heteropolyacid fluidized system

Shuangmei Han [a], Xiaolei Zhang [c], Ruizhen Wang [a], Kui Wang [a,b], Jianchun Jiang [a,b], , Junming Xu [a,b]*

[a] *Institute of Chemical Industry of Forest Products, Chinese Academy of Forestry; Key Lab. of Biomass Energy and Material, Jiangsu Province; National Engineering Lab. for Biomass Chemical Utilization, Nanjing 210042, China*

[b] *Co-Innovation Center of Efficient Processing and Utilization of Forest Resources, Nanjing Forestry University, Nanjing 210037, China*

[c] *Department of Chemical and Process Engineering, University of Strathclyde, Glasgow G1 1XJ, U.K.*

*Corresponding author. Email adress: xujunming@icifp.cn

Abstract

The electrocatalytic hydrodeoxygenation (ECH) of lignin typical model compounds and lignin-derived oil from different tree species into (alkyl)-cyclohexane and (alkyl)-cyclohexanol in the fluidized electrocatalysis system were investigated in this research. The selected model compounds include two G-type compounds: eugenol (EO) and guaiacol (GO), and two S-type compounds: 4-allyl-2,6-dimethoxyphenol (4-DMP) and 2,6-dimethoxyphenol (2,6-DMP). This ECH system consisted of phosphotungstic acid (PW_{12}) electrolyte, catalyst that suspended in the electrolyte, and $NaBH_4$ reductant in the cathode. The results showed that 4-DMP could be converted using Pt/C as the

catalyst at 25 mA/cm^2 current density and 80 °C for 60 minutes, with higher faradaic efficiency of 90% and the selectivity of PCH and 4-PCH was 62% and 20%, respectively. ~~The possible mechanism of 4-DMP hydrodeoxygenation (HDO) in this system was also explored.~~ For C-O bond cleavage, the DFT calculations showed that, for EO, GO, and 4-DMP, the C-OCH$_3$ bond will be firstly broken, while for 2,6-DMP, it is preferred that C-OH bond will be firstly broken. It was found that G-type (EO, GO) was more easily hydrodeoxygenated than S-type (4-DMP, 2,6-DMP) compounds, with the reaction rate in an order of GO > EO > 2,6-DMP > 4-DMP, indicating that the allyl group had a negative effect on the electrocatalytic conversion. Furthermore, it was also found that the complete conversion of lignin-derived oil monomers of pine (mainly G-type) and poplar (mainly S-type) can be achieved, with the yield of target products (PCH and 4-PCH) of 64% and 43%, respectively. Overall, this work innovatively integrates biomass refining and electrocatalytic upgrading, that provides a green and environmentally friendly solution for lignin conversion and utilisation.

Keywords: Fluidized electrocatalytic system, NaBH$_4$, ECH, G-type, S-type, C-O bond cleavage.

1. Introduction

Converting biomass into hydrocarbon fuels and chemicals has recently attracted much attention as one of the solutions to address the challenges of fossil fuels shortage and climate change [1-3]. Within the three components of biomass (cellulose, hemicellulose, and lignin), lignin is the second-largest (after cellulose) with an annual production of 70 million tons globally [4]. When compared with cellulose and

hemicellulose, lignin is rich in aromatic compounds with high chemical value [5-7] thus upgrading technologies can be developed to convert lignin into fuels and chemicals and avoiding it to be burned [5, 8, 9]. The typical lignin upgrading method is catalytic depolymerization to produce small molecular weight lignin-derived oil [10, 11], which can be further hydrodeoxygenated into high-quality fuel and chemicals by reducing the high oxygen content of unsaturated aromatic compounds in the lignin-derived oil [12-14].

In recent years, there have been many studies on hydrodeoxygenation (HDO) of lignin-derived phenolic compounds to produce hydrocarbons through thermochemical catalytic hydrogenation (TCH) [15-17]. However, this process typically requires relatively high temperature (200-500 °C) and high pressure (H_2 pressure > 20 bar) [18-20]. This high temperature often led to the polymerization of phenolic compounds and coke formation. Therefore, it is necessary to find a way to achieve HDO of unsaturated aromatic compounds under mild conditions.

Electrocatalysis is a clean, mild, and efficient conversion technology. During electrocatalysis, the electricity generated from renewable energy (such as solar and wind energy) can be converted into chemical energy [21-24] (**Scheme 1**). Compared to TCH, electrocatalytic hydrogenation (ECH) could achieve efficient conversion of substrates under mild conditions (temperature below 100 °C, atmospheric pressure) [25, 26]. The reaction rate and selectivity of electrolytic products could be controlled by adjusting the current and potential [21, 27].

Using ECH to upgrade lignin-derived phenolic compounds into cyclohexane

products and KA oil (cyclohexanol and cyclohexanone products) has been investigated by fixing the selected catalysts on the electrode [1, 2, 28]. Saffron and co-workers [29] used ruthenium supported on activated carbon cloth (Ru/ACC) in hydrochloric acid electrolyte for electrocatalytic hydrogenation of 2,6-dimethoxyphenol (2,6-DMP). They have obtained five products including cyclohexanol with a conversion rate of 58% and a faradaic efficiency of 29%. However, these electrocatalytic systems need to be further improved to solve the problems of low faradaic efficiency (20-60%) [30-32] and shedding of catalysts attached to the electrode [33, 34].

Instead of fixing the catalyst on the electrode, dispersing the catalyst in the electrolyte might solve the problem. For example, Liu Wei [35] and his co-workers reported a fluidized electrocatalytic system with silicotungstic acid (SiW_{12}) as cathode electrolyte, dispersed the catalyst in the electrolyte, and finally generated cyclohexane and cyclohexanol products with high faradaic efficiency (> 90%). They used guaiacol as a model compound for ECH. Under 100 mA/cm^2 for 25 minutes, guaiacol was completely converted to cyclohexane and cyclohexanol with the selectivity of 50.2% and 17.4%, respectively. However, the process required a long pre-electrolysis time (30 minutes). Furthermore, with the increment number of chemical groups in phenolic compounds, especially the influence of 2, 4, 6 substituents, the reduction is more difficult, which was also reported by Saffron et al. [29].

Lignin consisted of various phenolic compounds with multiple substituents. Typical phenolic compounds from different tree species usually contain S-type and G-type [36-39]. G-type phenolic compounds are originated from softwood tree species, e.g., pine

[40], camphorwood [41], and Cunninghamia lanceolata [42]. S-type phenolic compounds are originated from hardwood tree species, e.g., poplar [43], beech [44], and birch [45]. The major difference between G-type and S-type phenolic compounds is the amount of methoxy groups. G-type phenolic compounds have one methoxy group located next to the phenolic hydroxyl group, and S-type phenolic compounds have two methoxy groups located on both sides of the phenolic hydroxyl group. During the electrocatalytic hydrogenation reaction, methoxy groups greatly affect the conversion of the substrates and reaction rate, which may contribute to steric hindrance and electronic effect [46]. Moreover, Allyl (or propyl) is located in the para position of the phenolic hydroxyl group, which may effluence the conversion of the substrate because of its conjugation effect [47].

In this research, the ECH of lignin model compounds and lignin-derived oil monomers from different tree species under mild conditions ($\leq$ 95 °C, atmospheric pressure) have been investigated. The lignin model compounds were carefully selected, including S-type compounds such as 4-allyl-2,6-dimethoxyphenol (4-DMP) and 2,6-dimethoxyphenol (2,6-DMP); and G-type compounds such as eugenol (EO) and guaiacol (GO). To reduce pre-electrolysis time, we proposed sodium borohydride (NaBH4) as a reductant and hydrogen supplier. We developed a heteropolyacid-based system with PW_{12} as cathode electrolyte, phosphate (H_3PO_4) as anode electrolyte, and Pt/C as catalyst suspended in the cathode electrolyte. Furthermore, we compared the reaction rates, internal energy, and bond dissociation energies (BDEs) of the G-type and S-type compounds and gave the possible mechanism of C-O bond cleavage of 4-DMP

and 2,6-DMP.

Scheme 1 A green and environmentally friendly lignin conversion pathway
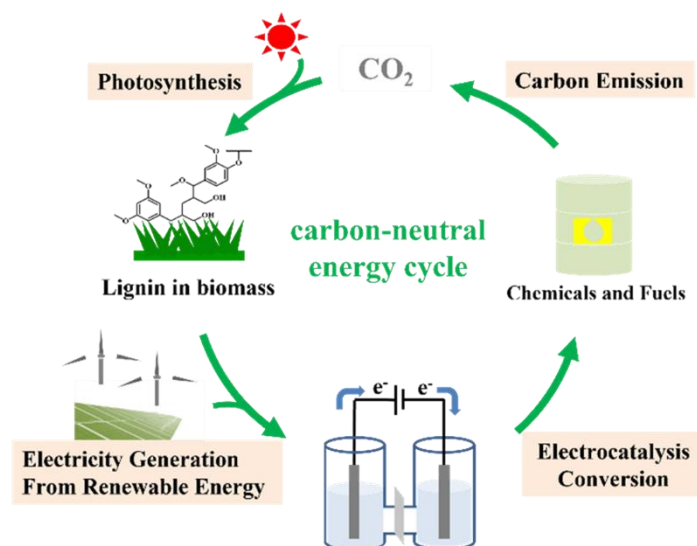
2. Materials and methods

2.1. Materials

All the materials to be used in the experiment were purchased from various sources, these materials include: the lignin model compounds (4-DMP, EO, GO, 2,6-DMP), electrolyte (PW_{12}, H_3PO_4), reductant ($NaBH_4$), catalysts (Pt/C, Pd/C, Rh/C, Ru/C), xxx. In detail, 4-DMP (AR, 98%) was purchased from Afaresha Chemical Co., Ltd. EO (AR, 99%), GO (AR, 99%), and 2,6-DMP (AR, 98%), PW_{12} (AR), n-hexane (AR, ≥ 97.0%) and methanol (AR, ≥ 99.5%) were obtained from Shanghai Maclin Biochemical Technology Co., Ltd. H_3PO_4 (AR, ≥ 85%), dichloromethane (CH_2Cl_2, AR, ≥ 99%) were obtained from Xilong Scientific Co., Ltd. Sodium borohydride ($NaBH_4$) was obtained from Shanghai Titan Chemical Co., Ltd. Hydrogen peroxide solution (H_2O_2, AR, 30 wt.% in H_2O) was obtained from Aladdin Industrial Corporation. Pt/C (5 wt.%), Pd/C (5 wt.%), Rh/C (5 wt.%), Ru/C (5 wt.%) were obtained from Sigma Company in USA.

Poplar and pine sawdust were obtained from Nanjing Province of China and the mech powder of 60-120 were selected and further pretreated by overnight drying at 105 °C to reach a constant weight. "H" shaped electrolytic cell was purchased from Hangzhou Saiao Electrochemical Experimental Equipment Co., Ltd. Electrochemical workstation was purchased from Shanghai Chenhua Instrument Co., Ltd.

2.2. Electrolysis of lignin-derived model compounds (4-DMP, EO, GO, and 2,6-DMP)

An "H" shaped cell (**Fig. 1**) was used with a graphite rod as the working electrode, a platinum plate (2×2cm) as the anode electrode, and Ag/AgCl as the reference electrode. 3% H_2O_2 aqueous solution was added to the electrolytic cell one day before to …. 11 mL 0.25 M PW_{12} solution and 2 M H_3PO_4 solution were added to the cathode and anode electrolytic chamber, respectively. Before the electrolysis reaction, 10 mM model compound, 0.4 g $NaBH_4$, and 0.05 g catalyst were added and maintained at a constant current (0-75 mA/cm^2). The electrolysis reaction was then started at a constant temperature with 600 rpm. After the electrolysis, the electrolyte was cooled down to room temperature, and the electrolytic products were extracted with CH_2Cl_2.

The supernatant liquid was used for quantitative gas chromatography (GC, Agilent 2010 Plus) and qualitative analysis by gas chromatography-mass spectrometry (GC-MS, QP2010 Ultra). The inlet temperature was 250 °C, the carrier gas was high purity helium, and the flow rate was 2.50 ml/min. The heating program was set as keeping at 50 °C for 2 minutes and further rising to 280 °C at 10 °C/min for 10 minutes. Ion source temperature was 230 °C, solvent removal time was 3 minutes, interface temperature was 280 °C, and scanning m/z was 45-500.
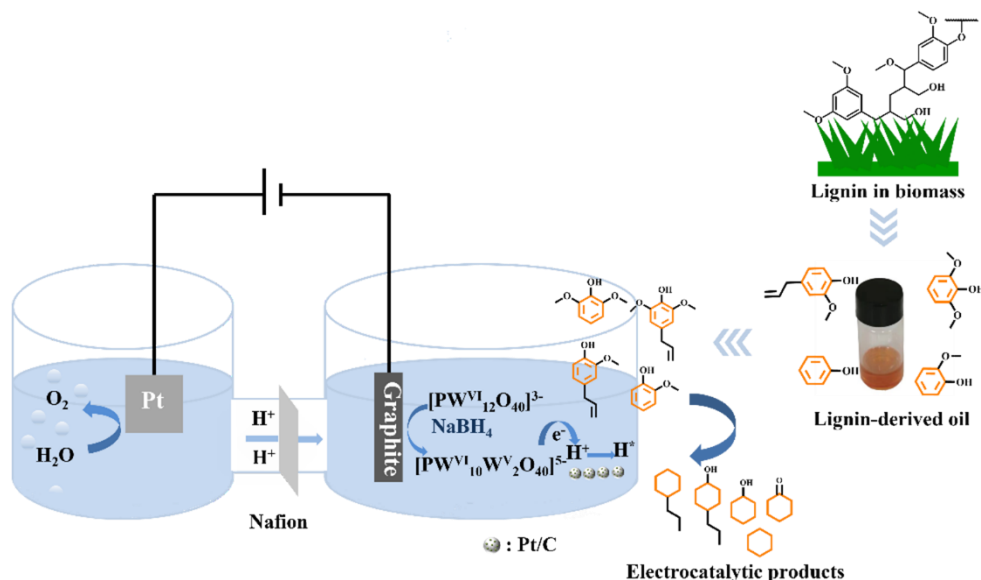
Fig. 1. Schematic diagram of fluidized electrocatalysis with PW_{12} as electron transfer carrier, $NaBH_4$ as reductant and hydrogen supplier.

2.3. Preparation and electrolysis of lignin-derived oil monomers

Preparation of lignin-derived oil monomers can be referred to the method in the previous literature [48]. Firstly, 60-120 mesh poplar or pine sawdust (2g), methanol (30 ml), Ru/C catalyst (0.4 g), and 3 MPa H_2 were added into a 50 ml reactor. The reaction was proceeded at 245 °C for 6 hours with a stirring rate of 1000 rpm. After the reaction, the obtained mixture was filtered to separate the residue part and the liquid part. The residue part was washed several times using methanol to ensure there is no lignin oil in the residue. The filtered liquid was evaporated by rotary evaporation at a temperature of 60 °C; 20 mL CH_2Cl_2 and 20 mL deionized water was added and poured into the separator funnel for extraction. The layer liquid was taken, and rotary evaporation was performed at 40 °C to remove CH_2Cl_2. The lignin-derived oil was then obtained. To separate the lignin-derived oil monomers from lignin-derived oil, n-hexane (with a

mass five times of that of lignin-derived oil) was added to the lignin-derived oil for reflux extraction at 80 °C for 3 hours. The above operation was repeated three times. Finally, the lignin-derived oil monomers were obtained by rotary evaporation of n-hexane at 60 °C. Regarding the electrolysis of lignin-derived oil monomers, similar operations were performed to the ECH and analysis methods of the model compounds (4-DMP, EO, GO and 2,6-DMP) as listed in Section 2.2.

2.4. Catalyst characterization

Transmission electron microscope (TEM) images were measured using FEI Talos F200X to characterize the catalyst morphology at 200 kV acceleration voltage with 520 mm camera length, 0.0251 A electronic wavelength, 0.25 nm point resolution, 0.12 information resolution, and 0.16 nm STEM resolution. The BET specific surface area, average pore size, and pore volume of catalysts were determined by the N_2 absorption method with a 20s equilibration interval at -196 °C on Micromeritics Tristar II 3020 apparatus. H_2 temperature-programmed desorption (H_2-TPD) was measured on Micromeritics AutoChem II 2920 apparatus. X-ray photoelectron spectra (XPS) was performed on Thermo Scientific K-Alpha. The AlKα ray (hv=1486.6 eV) was used as excitation source, and the Avantage software was used for peak fitting and calibration.

2.5. Calculations

The conversion, selectivity, yield, current density, reaction rate, and faradaic efficiency (F.E.) were calculated according to Equations 1-6, respectively.

Conversion (%)

= ((Initial moles of substrate (mol) - Final moles of substrate (mol)) / Initial moles

of substrate (mol)) × 100%   *Equation 1*

Selectivity (%)

= (Moles of target product (mol) / ΣMoles of all products (mol)) × 100%

Equation 2

Yield (%)

= (Moles of target product (mol) / Initial moles of substrate (mol)) × 100%

Equation 3

Current density

= (Current (mA) / Surface area of graphite rod in contact with electrolyte (cm^2))

Equation 4

Reaction rate

= (Moles of substrate consumed (mmol) / (Time (s) × Mass of active metal in

added catalyst (g)))

Equation 5

F.E. (%)

= ((Moles of final products (mol) × n × 96485 (C mol^{-1})) / (I (A) × t (s)))× 100%

Equation 6

Where n is the number of reaction electrons.

2.6. Computational calculations

The detailed bond breaking mechanism was investigated based on density functional theory (DFT) using Gaussian 16W software. Firstly, the structure of the initial substrate was built, and then the structure was optimized by B3LYP/6-31G* basis set. After the

structure was optimized, it was split into several fragments, and similar optimization operations were performed on several fragments. Both the model structures and their split fragments are further optimized using a higher level (comparing with B3LYP/6-31G*) method and basis set basis set, M062X/def2TZVP. Bond dissociation energy (BDE) is the energy needed to break a bond in a molecule. The BDE was calculated using the sum of the energies of several fragments minus the energies of the total model. For example, for the bond breaking reaction R→S+T, the BDE = E (S) + E (T) – E (R).

3. Results and discussion

3.1. ECH performances of lignin-derived model compounds

This paper mainly used the 4-DMP model compound to represent S-type lignin for ECH studies. To investigate the ECH performance of 4-DMP, the effect of $NaBH_4$ amount, catalysts, reaction temperature, current density, and reaction time on the ECH of 4-DMP were studied. Meanwhile, the potential was recorded and the F.E. corresponding to different current densities in the reaction process was provided.

First, we used pre-electrolysis for ECH of 4-DMP. After pre-electrolysis at 100 mA/cm^2 for 30 minutes, 4-DMP and Pt/C were added for electrolysis at low current density (25 mA/cm^2) and high current density (175 mA/cm^2) for 15 minutes. Other conditions and operations were the same as those of the electrocatalysis with $NaBH_4$. The results showed that, for the pre-electrolysis without $NaBH_4$, the conversion of 4-DMP was 5.50% and 14.23%, for the low and high current density, respectively. The conversion increased significantly to 69.68% and 99.99% after the addition of $NaBH_4$, indicating that the electrocatalytic efficiency of PW_{12} by pre-electrolysis was lower than

that by adding NaBH$_4$. Compared with the study that the ECH by pre-electrolysis at high current density (175 mA/cm^2) with low electrocatalytic efficiency, we achieved the efficient ECH of the substrate at low current density (25 mA/cm^2) using NaBH$_4$ (**Fig. 2**).
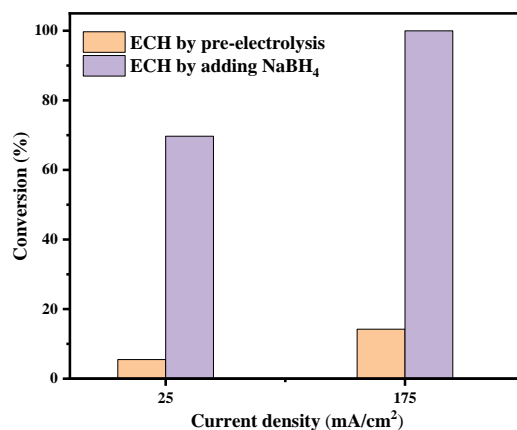

Fig. 2. ECH of 4-DMP by pre-electrolysis and adding NaBH$_4$ (at low and high current densities).

3.1.1. Effect of NaBH$_4$ amount on ECH of 4-DMP

NaBH$_4$ was used as reductant to reduce $[PW^{VI}_{12}O_{40}]^{3-}$ to $[PW^{VI}_{11}W^{V}O_{40}]^{4-}$ and $[PW^{VI}_{10}W^{V}_{2}O_{40}]^{5-}$. The initial PW$_{12}$ electrolyte solution was colorless and transparent (**Fig. 3a**). After adding NaBH$_4$ into the electrolyte, the solution immediately became dark-blue (**Fig. 3b**), indicating that PW$_{12}$ was rapidly reduced (re-PW$_{12}$). The amount of NaBH$_4$ was explored under the current density of 25 mA/cm^2, as shown in **Fig. 5a**. With the increase of the dosage of NaBH$_4$, the conversion of 4-DMP firstly increased and then decreased, from 11.64% to 69.68% and then decreased to 51.23%. It was found that 0.4 g NaBH$_4$ was the optimum amount for reducing PW$_{12}$. When the dosage of NaBH$_4$ was 0.3 g, the main products were PCH and 4-DMC with the selectivity of 52.02% and 26.07%, respectively, indicating that when PW$_{12}$ was not completely

reduced, the hydrogenation process accounted for a large proportion. As the amount of NaBH$_4$ increased to 0.4 g, the selectivity of 4-MP and 4-DMC decreased, and the selectivity of other products increased. The selectivity of 4-PCH increased from 3.33% to 14.68%, and there was no 4-MP in the final products. Although the selectivity of the final products with excessive NaBH$_4$ (0.45 g) was not significantly different from those at 0.4 g, however, the conversion was quite different, indicating that an appropriate amount of NaBH$_4$ could exactly reduce PW$_{12}$. This can be explained as the excessive NaBH$_4$ would consume H$^+$ in the electrolyte, resulting in the reduction of H* finally formed on the catalyst surface, thereby reducing the electrocatalytic efficiency.

The solution after the reaction was placed in the air for 15 days (ox-PW$_{12}$), and the solution was oxidized from dark-blue to dark-yellow (**Fig. 3c** and **Fig. 3d**). Put ox-PW$_{12}$ on the cathode and pumped current; the dark-yellow solution immediately turned dark-blue again (**Fig. 3c**), which showed that ox-PW$_{12}$ could still be reduced and had the same properties as untreated PW$_{12}$. To further explore whether ox-PW$_{12}$ can be reduced to the original PW$_{12}$ under energized conditions for further recycling, Current-Potential (CV) curve scans were performed on untreated PW$_{12}$, re-PW$_{12}$, ox-PW$_{12}$, and ox-PW$_{12}$ energized for 15 minutes (**Fig. 3e**). The redox potential of ox-PW$_{12}$ and ox-PW$_{12}$ energized for 15 minutes were similar to that of untreated PW$_{12}$, which was completely different from that of re-PW$_{12}$, which indicated that re-PW$_{12}$ could also be spontaneously oxidized to ox-PW$_{12}$ and then it can return to the same effect as untreated PW$_{12}$ with a small amount of current. This showed that PW$_{12}$ reduced by NaBH$_4$ had good recyclability.
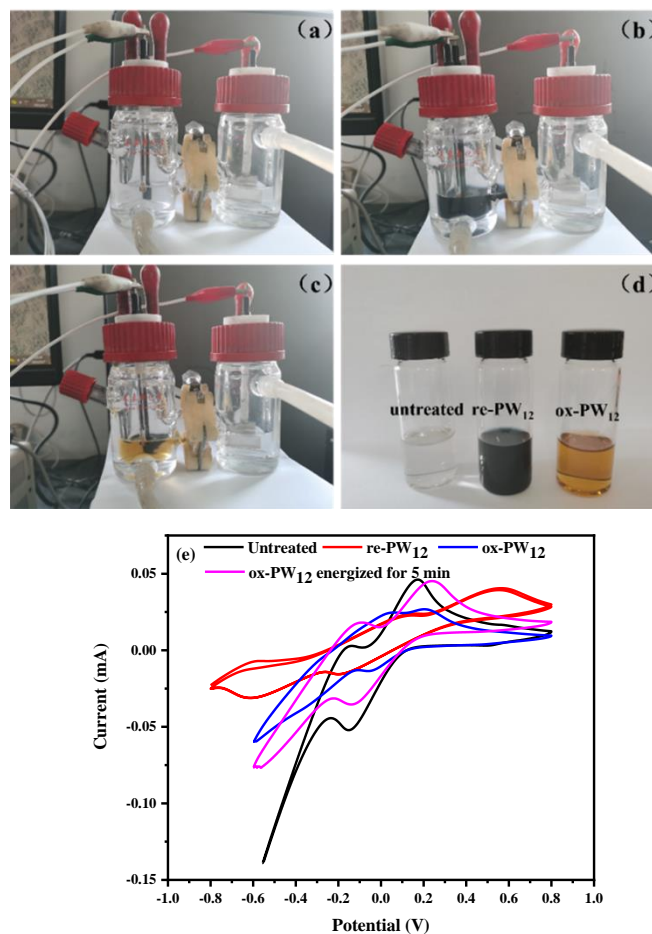
Fig. 3. The color change diagram of (a) PW_{12}, (b) re-PW_{12}, (c) ox-PW_{12}, and (d) ox-PW_{12}; and (e) the CV curve of PW_{12}, re-PW_{12}, ox-PW_{12}, ox-PW_{12} energized for 15 minutes.

3.1.2. Effect of catalysts on ECH of 4-DMP

Catalysts loaded with different metals had a great influence on the ECH. The catalytic performance of four different noble catalysts (Ru/C, Pd/C, Rh/C, and Pt/C) at 80 °C, 25 mA/cm^2 for 45 minutes was shown in **Fig. 4**. Compared with Ru/C, Pd/C and Rh/C, Pt/C showed better catalytic hydrogenation performance with the highest conversion of 88.07%, whereas the conversion of Ru/C (1.99%), Pd/C (8.53%) and Rh/C (6.28%) were all less than 10%. 4-n-propylphenol (4-PP) and 2-methoxy-4-(1-propyl)phenol (4-MP) were the main hydrogenation products under the action of Pd/C and Rh/C,

14

respectively. Among the obtained electrocatalytic hydrogenation products with Pt/C, propylcyclohexane (PCH) and 4-propylcyclohexanol (4-PCH) were the main products, and the selectivity was 65.86% and 16.79%, respectively. And there were some intermediate products, such as 4-propyl-2-methoxycyclohexane (4-MCH), 4-n-propylphenol (4-PP), 2-methoxy-4-(1-propyl)phenol (4-MP), 4-propyl-2,6-dimethoxycyclohexane (4-DMC). To further explore the catalytic activity of the Pt/C catalyst, BET (**Table S1** and **Fig. S1a**), H_2-TPD (**Fig. S1b**), TEM (**Fig. S2**) and XPS (**Fig. S3**) tests were performed on the catalysts.

From the BET and H_2-TPD results, Pt/C had a higher surface area and pore volume compared with Pd/C, Ru/C and Rh/C. Furthermore, Pt/C not only dissociated H_2 into active hydrogen (H^*) at lower temperatures (at about 120 ℃) and had the largest area of H_2 desorption peak, indicating that Pt/C catalyst had more active adsorption centers and a larger coverage, and then was more likely to promote the dissociation of H_2. From the TEM images, the particle size of the Pt/C catalyst (1.17 nm) was smaller than that of Pd/C (2.50 nm), Ru/C (8.01 nm) and Rh/C (5.59 nm). Meanwhile, the dispersion degree of metal nanoparticles in Pt/C was higher than that in Pd/C, Ru/C and Rh/C. From XPS results, two strong doublets at 71.2 eV and 74.5 eV binding energies for Pt/C indicated the presence of a large amount of metallic Pt^0 in **Fig. S3d**, consistent with previous literature [49, 50]. The chemical content and structures of the other three catalysts (Rh/C, Ru/C and Pd/C) were also annotated according to the literatures [51-54], details of the four catalysts were shown in **Table S2**.

The difference in the efficiency of catalysts loaded with different metals might be

due to the physicochemical properties and the lower ability of the platinum metal surface to bind hydrogen [55], which was helpful for the combination of the substrate with H[*] and the promotion of ECH conversion.
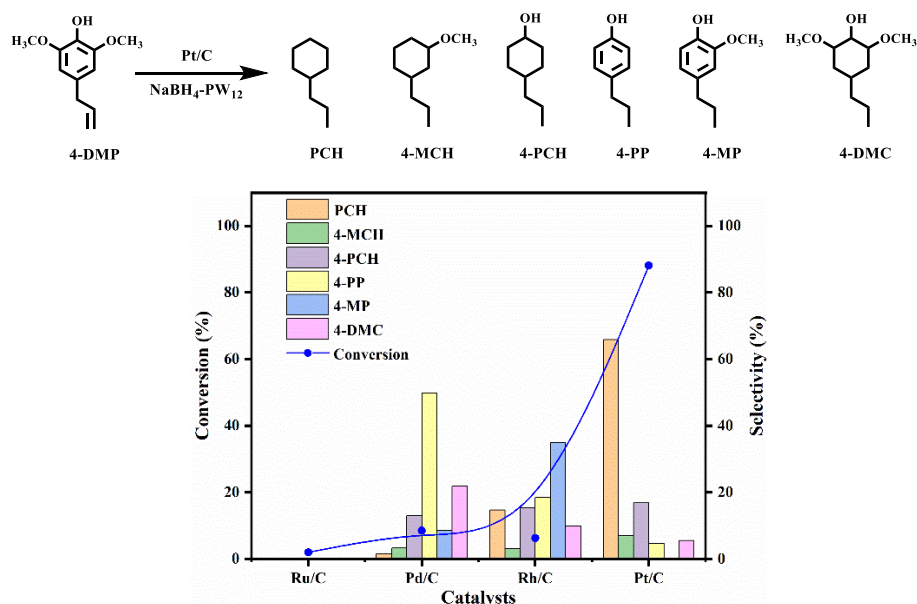
Fig. 4. Distribution of conversion products of 4-DMP over different supported metal catalysts. Reaction conditions: 10 mM substrate, 0.40 g NaBH$_4$, 25 mA/cm^2, 80 ℃, 45 minutes.

3.1.3. Effect of current density on ECH of 4-DMP

Fig. 5b showed the conversion of 4-DMP and selectivity of electrocatalytic products under different current densities (0-75 mA/cm^2). When the current density is 0 mA/cm^2, 25 mA/cm^2, 50 mA/cm^2 and 75 mA/cm^2, the potential is -0.2 V, -0.4 V, -0.6 V and -0.8 V, respectively. As the current density increased from 0 to 75 mA/cm^2, the conversion increased from 19.98% to 99.98%, which was due to the more formation of H[*] that promotes the conversion of the substrate at higher current. The selectivity of 4-PCH increased from 4.75% to 21.54%, and the selectivity of PCH increased from 43.71% to about 60% and remained stable. The reaction rate decreased with increasing current

16

density, which may be due to the HER at higher current densities.

At the current density of 0 mA/cm^2, the conversion of 4-DMP was 19.89%, which indicated that NaBH$_4$ acted as a reductant in the system and acted as a hydrogen supplier to provide a hydrogen source to promote the reaction. PCH and 4-DMC were the main products, indicating that thermochemical catalysis of 4-DMP was mainly for hydrogenation (allyl double bond hydrogenation and phenyl ring hydrogenation) and complete HDO to form PCH without providing current. The F.E. at 25-75 mA/cm^2 was calculated to be 90.46%, 80.8%, and 77.41%, respectively.

3.1.4. Effect of reaction temperature on ECH of 4-DMP

The effect of temperature on the HDO of 4-DMP was shown in **Fig. 5c**. When the reaction temperature increased from 50 ℃ to 80 ℃, the conversion of 4-DMP rose from 28.71% to 69.68%. The selectivity of PCH increased from 40.97% to 59.56%, and the selectivity of 4-DMC decreased to 10.07%. At the same time, 4-MP was not detected in the final products, indicating that the increase in temperature was conducive to the ECH reaction. However, with the temperature continued to rise to 95 ℃, the conversion of 4-DMP remained unchanged compared with that at 80 ℃. Meanwhile, compared with the previous studies on the effect of temperature on the electrocatalytic hydrogenation of 2-MP [56], indicating that the decrease of 4-DMP conversion required higher temperature. The reason for the decline in substrate conversion might be that high temperature accelerated HER [57], which was also proved by a previous report [58].

3.1.5. Effect of reaction time on ECH of 4-DMP

The conversion rate of 4-DMP and the selectivity of electrocatalytic products in the time range of 0-60 minutes were given (**Fig. 5d**). With the increase of time, the conversion of 4-DMP was from 40.23% to 96.92%. The selectivity of 4-PCH increased from 8.87% to 20.88%, while the selectivity of PCH increased slowly, indicating that PCH and 4-PCH may be obtained by different reaction pathways. When the reaction time was 60 minutes, the conversion rate of 4-DMP reached 96.92%, which was completely converted. The selectivity of the main products (PCH and 4-PCH) reached 84%. Meanwhile, 4-DMC was not detected in the products, indicating that the hydrogenation product (4-DMC) was more converted to the main products (PCH and 4-PCH) with time increasing.
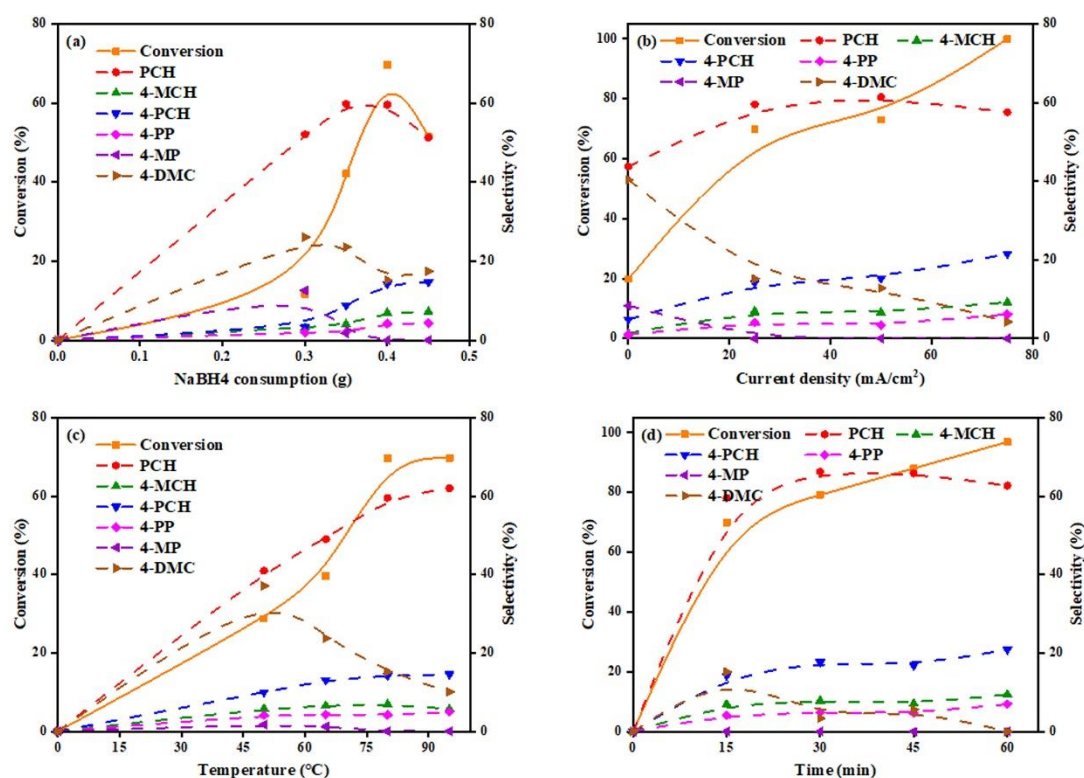
Fig. 5. (a) Distribution of electrocatalytic products of 4-DMP over different NaBH₄ consumption.

Reaction conditions: 10 mM substrate, Pt/C, 25 mA/cm², 80 °C, 15 min. (b) Distribution of
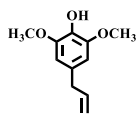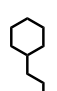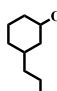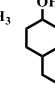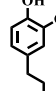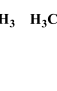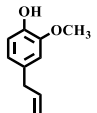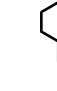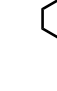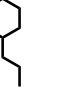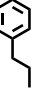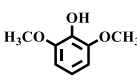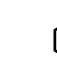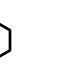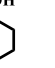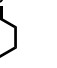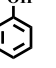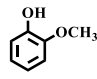
electrocatalytic products of 4-DMP over different current density. Reaction conditions: 10 mM substrate, Pt/C, 0.4 g NaBH$_4$, 80 °C, 15 min. (c) Distribution of electrocatalytic products of 4-DMP over different temperature. Reaction conditions: 10 mM substrate, Pt/C, 0.4 g NaBH$_4$, 25 mA/cm^2, 15 min. (d) Distribution of electrocatalytic products of 4-DMP over different reaction time. Reaction conditions: 10 mM substrate, Pt/C, 0.4 g NaBH$_4$, 25 mA/cm^2, 80 °C.

3.1.6. ECH of EO, GO, and 2,6-DMP

To better explore the effect of groups on 4-DMP and the mechanism of bond cleavage, we performed ECH of GO, EO, and 2,6-DMP model compounds. The conversion, selectivity, and reaction rate of the four model compounds were shown 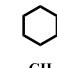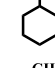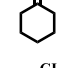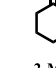in **Table 1**. The conversion of 4-DMP, 2,6-DMP, EO and GO were 40.23%, 54.12%, 68.38% and 75.25% under 25 mA/cm^2 for 10 minutes, respectively. The main products were PCH and 4-PCH for EO and 4-DMP. For GO and 2,6-DMP, the main electrocatalytic products were cyclohexane (CH) and cyclohexanol (CHL). The reaction rate of four model compounds was GO > EO > 2,6-DMP > 4-DMP, which showed that G-type compounds (GO and EO) were more accessible to perform HDO than S-type compounds (2,6-DMP and 4-DMP) in this electrocatalytic system. Under the same condition, the conversion without the allyl group (GO and 2,6-DMP) was higher than that with the allyl group (EO and 4-DMP), indicating that the allyl group had a negative effect on ECH.

Table 1 The conversion, selectivity, and reaction rate for four model compounds (10 mM substrates, 25 mA/cm^2, 80 °C, Pt/C, 10 min, 0.4 g NaBH$_4$).

Substrates	Conversion (%)	Products and selectivity (%)	Reaction Rate (mmol·s^{-1}·g^{-1})

Compound	Conversion	Products						BDE
4-DMP	40.23%	PCH 55.03%	4-MCH 2.99%	4-PCH 8.87%	4-PP 1.88%	4-MP 3.31%	4-DMC 21.06%	0.030
(EO)	68.38%	PCH 64.63%	4-MCH 3.07%	4-PCH 17.41%	4-PP 2.68%	4-MCHL 3.85%		0.050
(GO)	54.12%	CH 32.21%	CHL 20.03%	CHE 13.87%	PH 3.83%	2-MCO 19.32%		0.039
(2,6-DMP)	75.25%	CH 41.54%	CHL 14.87%	CHE 29.13%	2-MCO 13.11%			0.055

3.2. Comparison of the C-O bonds cleavage pathways of ECH in G-type and S-type compounds

To compare the C-O bonds cleavage order of the G-type and S-type compounds, the internal energies of the four model compounds and the BDEs of the C-OH and C-OCH$_3$ bonds were calculated by DFT (**Table 2**).

For 4-DMP, EO, and GO, the order of cleavage of the C-O bond tended to break the -OCH$_3$ group first, followed by the -OH group. The difference was that 2,6-DMP tended to break the -OH group first. This could be caused by: 4-DMP and EO had an allyl double bond, the -OCH$_3$ group and allyl group were in the meta position, and the -OH group and allyl group were in the para position. For the meta position, the conjugation effect was blocked, only the induction effect, which made the -OCH$_3$ group activated, the polarity became larger, and it was easier to leave; for the -OH group, there were conjugation effect and induction effect, the electron cloud density increased, the -OH
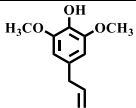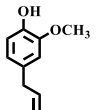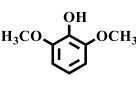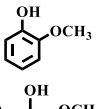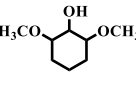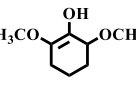
group was not easy to leave. For 2,6-DMP, without the influence of allyl group, the -OCH$_3$ group had σ-p hyperconjugation, and the -CH$_3$ group donated electrons to O, which increased the electron cloud density and strong bond of the -OCH$_3$ group. Therefore, the -OCH$_3$ group was not easy to leave, and the -OH group left first [59]. For GO, compared with 2,6-DMP, there was only one methoxy group, and the σ-p hyperconjugation was not as strong as 2,6-DMP, resulting in preferential cleavage of the -OCH$_3$ group.

Under the action of H*, both the hydrogenation process and the C-O bond cleavage process of the model compound were performed. Combined with the selectivity of the electrolysis product (2-MCO) of 2,6-DMP, which indicated that 2,6-DMP underwent hydrogenation process first, and then underwent the C-O bond cleavage process. The C–O bond cleavage priorities of the possible hydrogenation products (intermediate A and intermediate B) of 2,6-DMP were calculated by DFT. From the calculation results, it could be seen that the hydrogenation products (A and B) both first broke the -OCH$_3$ group.

On the other hand, H* formed in the reaction can donate electrons to -OCH$_3$ and -OH groups. For 4-DMP and 2,6-DMP, there were two -OCH$_3$ groups and one -OH group with three C-O bonds competing electrons, while EO and GO had only two C-O bonds competing electrons, so the reaction rate of EO and GO was higher than that of 4-DMP and 2,6-DMP. For 4-DMP and 2,6-DMP, the conjugation was elongated due to the presence of allyl in 4-DMP, and the electrons were delocalized, resulting in the electron cloud density of the C-O bond lower than that of 2,6-DMP, and the electrophilic

reactivity was lower. Therefore, the rate of 2,6-DMP was higher than that of 4-DMP,

the same as GO, which well explained the reaction rates of the four model compounds

that GO > EO > 2,6-DMP > 4-DMP as mentioned in section 3.1.6..

Table 2 The internal energy and bond dissociation energies (BDEs) of four model compounds.

Substrates	Internal energy (kJ·mol^{-1})	BDEs (kJ·mol^{-1})	
		a (-OCH$_3$)	b (-OH)
	-1.71×10^6	453.15	479.48
	-1.41×10^6	452.67	490.46
	-1.41×10^6	497.55	479.88
	-1.11×10^6	442.05	483.35
	-1.42×10^6	375.25	431.24
	-1.41×10^6	436.87 (a$_1$) 389.87 (a$_2$)	493.25
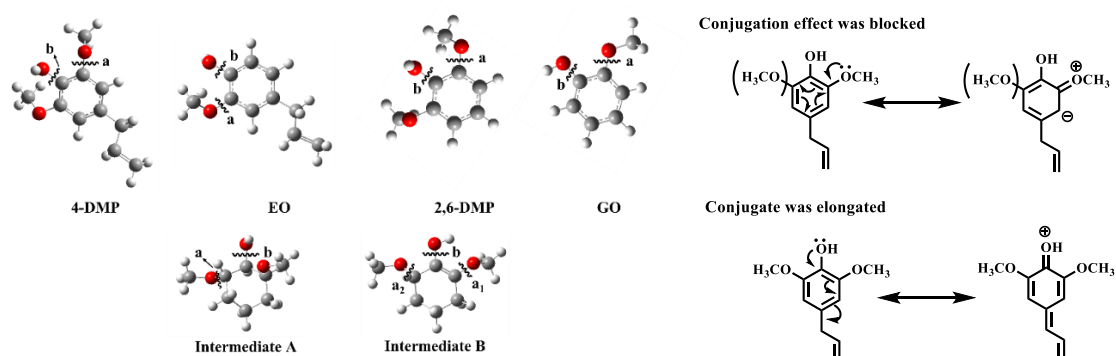
3.3. The possible ECH reaction pathways of 4-DMP and 2,6-DMP

Under the fluidized electrocatalysis system, NaBH$_4$ was used as a reductant to reduce

PW$_{12}$. Re-PW$_{12}$ functioned as an electron transfer carrier, which could transfer electrons

to the catalyst's surface and combine with H^+ to form H^*, promoting HDO of substrates.

Fig. 6 showed all possible C-O bond cleavage and hydrogenation pathways for 4-DMP and 2,6-DMP.

For 4-DMP, the first route was preferential cleavage of the -OCH_3 group, the second route was preferential hydrogenation and the third route was preferential cleavage of the -OH group. When the reaction time of 10 minutes, the main products were PCH and 4-DMC, with the selectivity of 55.03% and 21.06%, respectively. Meanwhile, according to the DFT calculation and analysis of the BDE of the C-O bond, 4-DMP preferentially cleaved -OCH_3 group. It showed that the primary reaction of 4-DMP was route 1, accompanied by side reactions (hydrogenation reaction, route 2). With the increase in reaction time, the selectivity of 4-DMC gradually decreased to 0, indicating that it underwent C-O bond cleavage and transformed into other products. DFT calculation results showed that it was more inclined to the C path. The intermediate product 4-PP was obtained after removing methoxy by 4-MP. On the one hand, 4-PP was hydrogenated to receive the main product (4-PCH); on the other hand, 4-PP was dehydrated and then hydrogenated to obtain the main product (PCH). Since the selectivity of PCH did not increase significantly with the reaction time, to explore whether 4-PCH was further converted into PCH, using 4-PCH as the substrate to conduct ECH research. The results showed that 4-PCH did not further remove the -OH group to convert into PCH, indicating that the main products (PCH and 4-PCH) were obtained through different reaction pathways.

For 2,6-DMP, the selectivity of the products (CH, CHL and CHE) increased with

time, while the selectivity of PH and 2-MCO decreased (**Table S3**). Combined with the

above analysis, 2,6-DMP preferentially broke the -OH group. Based on this, the

possible ECH pathways for 2,6-DMP were given. 2,6-DMP was almost completely

converted within 30 minutes of reaction, the selectivity of products (CH, CHL and CHE)

showed an overall upward trend, and the selectivity of PH and 2-MCO decreased with

time. The selectivity of 2-MCO reached 28.48% at 5 minutes, which indicated that the

HDO process of 2,6-DMP was more inclined to the hydrogenation route of benzene

ring (route 1), and then the -OCH$_3$ group was removed to generate the products (2-

MCO, CHE, CHL and CH). Certainly, this process was accompanied by the route 2.
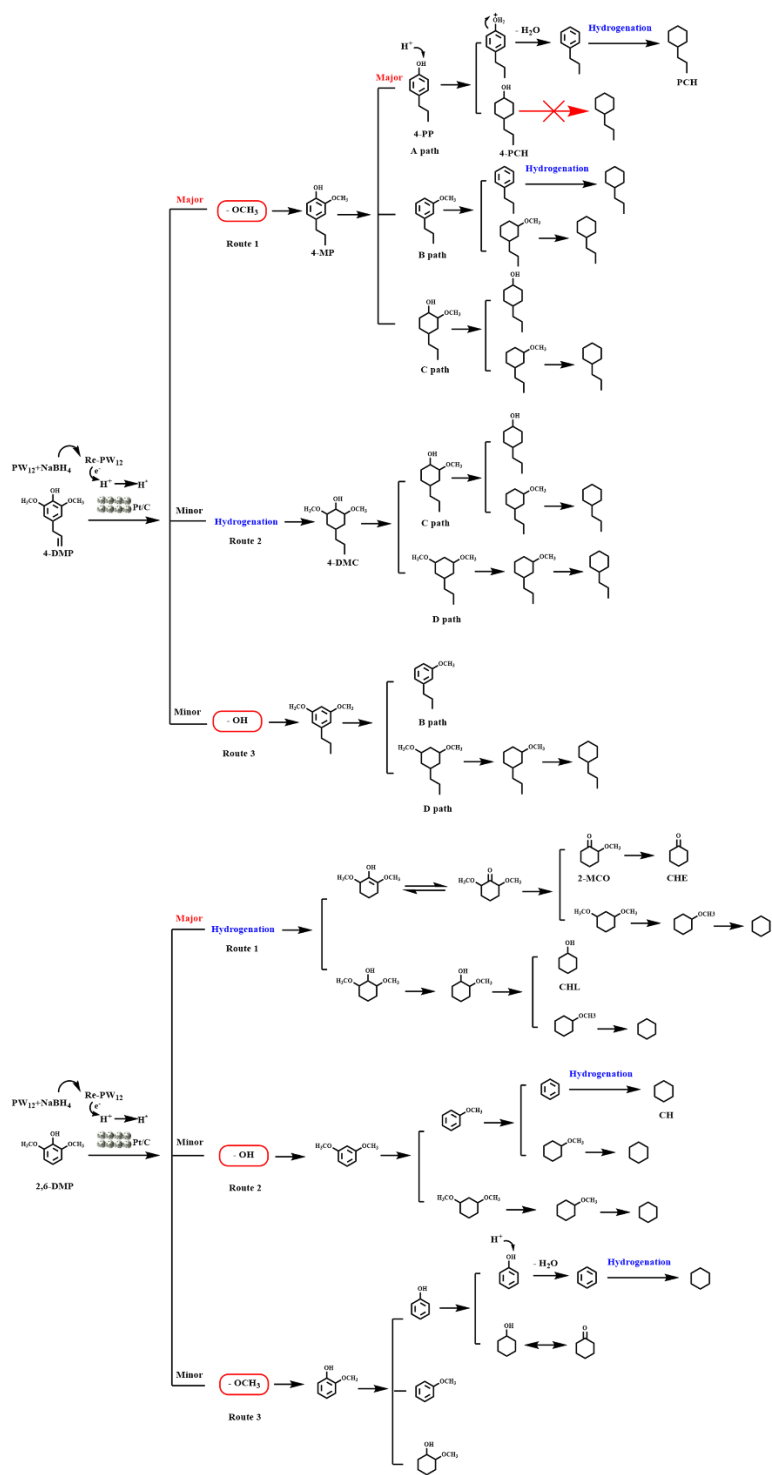
Fig. 6. Bond cleavage and hydrogenation routes of 4-DMP and 2,6-DMP.

3.4. ECH of lignin-derived oil

To investigate the applicability of this system to lignin-derived oil of different tree

species, ECH of lignin-derived oil monomers that obtained from catalytic

hydrogenation of poplar (mainly S-type) and pine (mainly G-type) at high current densities was studied. The mass yield of lignin-derived oil and lignin-derived oil monomers was calculated after n-hexane extraction. The mass yield of poplar lignin-derived oil was 21.05%, and the mass yield of poplar lignin-derived oil monomers was 49.51%. From the results of GC and GC-MS, 4-MP and 4-propyl-2,6-dimethoxyphenol (4-PDMP) were the main components of poplar lignin-derived oil monomers. Unlike poplar, 4-MP was the main component of pine lignin-derived oil monomers. The mass yield of pine lignin-derived oil was 19.38%, and the mass yield of pine lignin-derived oil monomers was 55.16% (**Fig. 7**).

The ECH of poplar (S-type) and pine (G-type) lignin-derived oil monomers was explored by reacting at different current densities (50-150 mA/cm^2) for different time (1-4 h). The results showed that 4-MP could be converted at low current density and short time, while 4-PDMP needed relatively harsh conditions. This was due to the existence of two -OCH_3 groups in 4-PDMP, resulting in low conversion efficiency of 4-PDMP, which was consistent with our above discussion. Under high current density (150 mA/cm^2), 4-PDMP of poplar lignin-derived oil monomers can be completely converted by electrochemical hydrogenation for 4 h. The yield of the target products (PCH and 4-PCH) was 43.28%, as shown in **Fig. 8a**. 4-MP of pine lignin-derived oil monomers reacted for 1 h at a low current density (50 mA/cm^2) with the conversion of 96%, and the yield of the target products (PCH and 4-PCH) was 64.35% (**Fig. 8b**), which also proved that 4-MP was more accessible to transform than 4-PDMP.
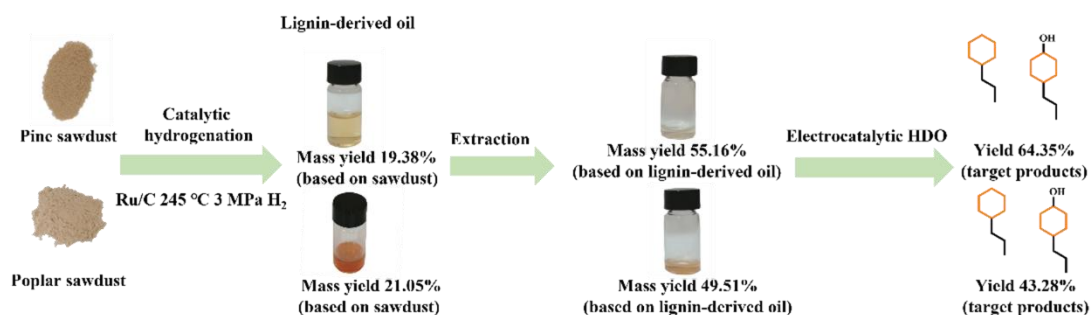
Fig. 7. ECH of lignin-derived oil monomers from different tree species.
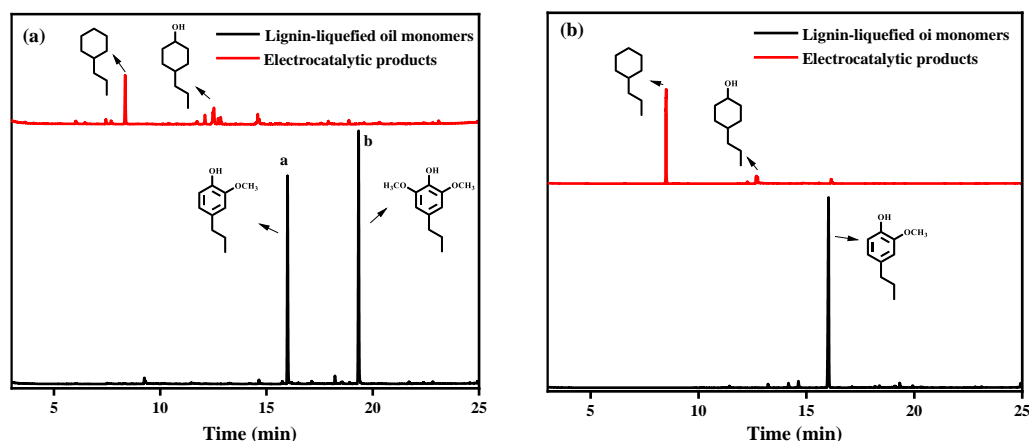
Fig. 8. GC Spectral of lignin-derived oil monomers from poplar (a), pine (b), and electrocatalytic hydrogenation products (a: 4-MP, b: 4-PDMP).

4. Conclusion

In this study, a fluidized electrocatalytic system dispersing Pt/C in PW_{12} solution under mild conditions ($\leq$ 95 °C, atmospheric pressure) was investigated and it has achieved efficient HDO for typical lignin phenolic compounds (G-type and S-type) from different tree species and lignin-derived oils. The selectivity of the main products (PCH and 4-PCH) in the ECH of 4-DMP was 62% and 20%, with high F.E. > 90%. For the S-type model compounds (4-DMP and 2,6-DMP), 4-DMP tended to remove $-OCH_3$ first followed by the hydrogenation pathway; 2,6-DMP preferred the hydrogenation process, accompanied by the -OH removal. Furthermore, the lignin-derived oil could also achieve ECH at high current densities with a high yield of PCH and 4-PCH

products, which provided a good reference for exploring the electrocatalysis of lignin-derived oil from different tree species. In conclusion, this work effectively applied electrocatalysis to convert phenolic compounds from different tree species into hydrocarbons and chemicals, which had excellent prospects in the area of lignin and biomass valorization.

Conflict of interest statement

The author states that the work has no interest in others.

Acknowledgments

References

[1] M. Garedew, D. Young-Farhat, J.E. Jackson, C.M. Saffron, Electrocatalytic Upgrading of Phenolic Compounds Observed after Lignin Pyrolysis, ACS Sustainable Chemistry & Engineering 7(9) (2019) 8375-8386. https://doi.org/10.1021/acssuschemeng.9b00019.

[2] C.H. Lam, C.B. Lowe, Z. Li, K.N. Longe, J.T. Rayburn, M.A. Caldwell, C.E. Houdek, J.B. Maguire, C.M. Saffron, D.J. Miller, J.E. Jackson, Electrocatalytic upgrading of model lignin monomers with earth abundant metal electrodes, Green Chemistry 17(1) (2015) 601-609. https://doi.org/10.1039/c4gc01632g.

[3] J.S. Luterbacher, D. Martin Alonso, J.A. Dumesic, Targeted chemical upgrading of lignocellulosic biomass to platform molecules, Green Chem. 16(12) (2014) 4816-4838. https://doi.org/10.1039/c4gc01160k.

[4] D.S. Bajwa, X. Wang, E. Sitz, T. Loll, S. Bhattacharjee, Application of bioethanol derived lignin for improving physico-mechanical properties of thermoset biocomposites, Int J Biol Macromol 89 (2016) 265-72. https://doi.org/10.1016/j.ijbiomac.2016.04.077.

[5] C. Chio, M. Sain, W. Qin, Lignin utilization: A review of lignin depolymerization from various aspects, Renewable and Sustainable Energy Reviews 107 (2019) 232-249. https://doi.org/10.1016/j.rser.2019.03.008.

[6] L. Dai, W. Zhu, J. Lu, F. Kong, C. Si, Y. Ni, A lignin-containing cellulose hydrogel for lignin fractionation, Green Chemistry 21(19) (2019) 5222-5230. https://doi.org/10.1039/c9gc01975h.

[7] J. Xu, C. Li, L. Dai, C. Xu, Y. Zhong, F. Yu, C. Si, Biomass Fractionation and Lignin Fractionation towards Lignin Valorization, ChemSusChem 13(17) (2020) 4284-4295. https://doi.org/10.1002/cssc.202001491.

[8] T.I. Koranyi, B. Fridrich, A. Pineda, K. Barta, Development of 'Lignin-First' Approaches for the Valorization of Lignocellulosic Biomass, Molecules 25(12) (2020).

https://doi.org/10.3390/molecules25122815.

[9] M.D. Cannatelli, A.J. Ragauskas, Laccase-mediated synthesis of lignin-core hyperbranched copolymers, Appl Microbiol Biotechnol 101(16) (2017) 6343-6353. https://doi.org/10.1007/s00253-017-8325-2.

[10] S. Van den Bosch, W. Schutyser, S.F. Koelewijn, T. Renders, C.M. Courtin, B.F. Sels, Tuning the lignin oil OH-content with Ru and Pd catalysts during lignin hydrogenolysis on birch wood, Chem Commun (Camb) 51(67) (2015) 13158-61. https://doi.org/10.1039/c5cc04025f.

[11] T. Aro, P. Fatehi, Production and Application of Lignosulfonates and Sulfonated Lignin, ChemSusChem 10(9) (2017) 1861-1877. https://doi.org/10.1002/cssc.201700082.

[12] S. Kim, E.E. Kwon, Y.T. Kim, S. Jung, H.J. Kim, G.W. Huber, J. Lee, Recent advances in hydrodeoxygenation of biomass-derived oxygenates over heterogeneous catalysts, Green Chemistry 21(14) (2019) 3715-3743. https://doi.org/10.1039/c9gc01210a.

[13] H. Duan, J. Dong, X. Gu, Y.K. Peng, W. Chen, T. Issariyakul, W.K. Myers, M.J. Li, N. Yi, A.F.R. Kilpatrick, Y. Wang, X. Zheng, S. Ji, Q. Wang, J. Feng, D. Chen, Y. Li, J.C. Buffet, H. Liu, S.C.E. Tsang, D. O'Hare, Hydrodeoxygenation of water-insoluble bio-oil to alkanes using a highly dispersed Pd-Mo catalyst, Nat Commun 8(1) (2017) 591. https://doi.org/10.1038/s41467-017-00596-3.

[14] Z. Yang, B. Luo, R. Shu, Z. Tian, Y. Kang, Y. Chen, Efficient hydrodeoxygenation of phenolic compounds and raw lignin-oil under a temperature-controlled phase-transfer catalysis, Fuel 291 (2021). https://doi.org/10.1016/j.fuel.2020.120091.

[15] N. Li, X. Zhang, Q. Zhang, L. Chen, Y. Li, C. Wang, L. Ma, Mo-based catalyst for chemical looping deoxygenation of phenolic compounds to aromatic hydrocarbons, Fuel Processing Technology 221 (2021). https://doi.org/10.1016/j.fuproc.2021.106936.

[16] P. Sirous-Rezaei, Y.-K. Park, Catalytic hydropyrolysis of lignin: Suppression of coke formation in mild hydrodeoxygenation of lignin-derived phenolics, Chemical Engineering Journal 386 (2020). https://doi.org/10.1016/j.cej.2019.03.224.

[17] D. Raikwar, M. Munagala, S. Majumdar, D. Shee, Hydrodeoxygenation of guaiacol over Mo, W and Ta modified supported nickel catalysts, Catalysis Today 325 (2019) 117-130. https://doi.org/10.1016/j.cattod.2018.09.039.

[18] M. Zhou, C. Chen, P. Liu, H. Xia, J. Li, B.K. Sharma, J. Jiang, Catalytic Hydrotreatment of β-O-4 Ether in Lignin: Cleavage of the C–O Bond and Hydrodeoxygenation of Lignin-Derived Phenols in One Pot, ACS Sustainable Chemistry & Engineering 8(38) (2020) 14511-14523. https://doi.org/10.1021/acssuschemeng.0c04941.

[19] M. Grilc, B. Likozar, J. Levec, Hydrodeoxygenation and hydrocracking of solvolysed lignocellulosic biomass by oxide, reduced and sulphide form of NiMo, Ni, Mo and Pd catalysts, Applied Catalysis B: Environmental 150-151 (2014) 275-287. https://doi.org/10.1016/j.apcatb.2013.12.030.

[20] J. Feng, Z. Yang, C.-y. Hse, Q. Su, K. Wang, J. Jiang, J. Xu, In situ catalytic hydrogenation of model compounds and biomass-derived phenolic compounds for bio-oil upgrading, Renewable Energy 105 (2017) 140-148. https://doi.org/10.1016/j.renene.2016.12.054.

[21] Y. Zhou, G.E. Klinger, E.L. Hegg, C.M. Saffron, J.E. Jackson, Multiple Mechanisms Mapped in Aryl Alkyl Ether Cleavage via Aqueous Electrocatalytic Hydrogenation over Skeletal Nickel, J Am Chem Soc 142(8) (2020) 4037-4050. https://doi.org/10.1021/jacs.0c00199.

[22] C.H. Lam, S. Das, N.C. Erickson, C.D. Hyzer, M. Garedew, J.E. Anderson, T.J. Wallington, M.A. Tamor, J.E. Jackson, C.M. Saffron, Towards sustainable hydrocarbon fuels with biomass fast pyrolysis oil and electrocatalytic upgrading, Sustainable Energy & Fuels 1(2) (2017) 258-266.

https://doi.org/10.1039/c6se00080k.

[23] H. Oh, Y. Choi, C. Shin, T.V.T. Nguyen, Y. Han, H. Kim, Y.H. Kim, J.-W. Lee, J.-W. Jang, J. Ryu, Phosphomolybdic Acid as a Catalyst for Oxidative Valorization of Biomass and Its Application as an Alternative Electron Source, ACS Catalysis 10(3) (2020) 2060-2068. https://doi.org/10.1021/acscatal.9b04099.

[24] W. Liu, C. Liu, P. Gogoi, Y. Deng, Overview of Biomass Conversion to Electricity and Hydrogen and Recent Developments in Low-Temperature Electrochemical Approaches, Engineering 6(12) (2020) 1351-1363. https://doi.org/10.1016/j.eng.2020.02.021.

[25] Y.P. Wijaya, K.J. Smith, C.S. Kim, E.L. Gyenge, Electrocatalytic hydrogenation and depolymerization pathways for lignin valorization: toward mild synthesis of chemicals and fuels from biomass, Green Chemistry 22(21) (2020) 7233-7264. https://doi.org/10.1039/d0gc02782k.

[26] X. Du, H. Zhang, K.P. Sullivan, P. Gogoi, Y. Deng, Electrochemical Lignin Conversion, ChemSusChem 13(17) (2020) 4318-4343. https://doi.org/10.1002/cssc.202001187.

[27] K. Li, Y. Sun, Electrocatalytic Upgrading of Biomass-Derived Intermediate Compounds to Value-Added Products, Chemistry 24(69) (2018) 18258-18270. https://doi.org/10.1002/chem.201803319.

[28] L. Li, L. Hu, J. Li, Z. Wei, Enhanced stability of Pt nanoparticle electrocatalysts for fuel cells, Nano Research 8(2) (2015) 418-440. https://doi.org/10.1007/s12274-014-0695-5.

[29] Z. Li, M. Garedew, C.H. Lam, J.E. Jackson, D.J. Miller, C.M. Saffron, Mild electrocatalytic hydrogenation and hydrodeoxygenation of bio-oil derived phenolic compounds using ruthenium supported on activated carbon cloth, Green Chemistry 14(9) (2012). https://doi.org/10.1039/c2gc35552c.

[30] Y. Song, O.Y. Gutiérrez, J. Herranz, J.A. Lercher, Aqueous phase electrocatalysis and thermal catalysis for the hydrogenation of phenol at mild conditions, Applied Catalysis B: Environmental 182 (2016) 236-246. https://doi.org/10.1016/j.apcatb.2015.09.027.

[31] Y. Jia, Y. Wen, X. Han, J. Qi, Z. Liu, S. Zhang, G. Li, Electrocatalytic degradation of rice straw lignin in alkaline solution through oxidation on a Ti/SnO2–Sb2O3/α-PbO2/β-PbO2 anode and reduction on an iron or tin doped titanium cathode, Catalysis Science & Technology 8(18) (2018) 4665-4677. https://doi.org/10.1039/c8cy00307f.

[32] S. Huang, X. Wu, W. Chen, T. Wang, Y. Wu, G. He, A bilateral electrochemical hydrogen pump reactor for 2-propanol dehydrogenation and phenol hydrogenation, Green Chemistry 18(8) (2016) 2353-2362. https://doi.org/10.1039/c5gc01719j.

[33] Y.-G. Zhou, Y. Kang, J. Huang, Fluidized Electrocatalysis, CCS Chemistry 2(1) (2020) 31-41. https://doi.org/10.31635/ccschem.020.201900065.

[34] A. Maljusch1, O. Conradi2, S. Hoch2, M. Blug2, W. Schuhmann1CA, Advanced Evaluation of the Long-Term Stability of Oxygen Evolution Electrocatalysts. %J Analytical Chemistry, (No.15) (2016) 7597-7602.

[35] W. Liu, W. You, Y. Gong, Y. Deng, High-efficiency electrochemical hydrodeoxygenation of bio-phenols to hydrocarbon fuels by a superacid-noble metal particle dual-catalyst system, Energy & Environmental Science 13(3) (2020) 917-927. https://doi.org/10.1039/c9ee02783a.

[36] A. Bhalla, N. Bansal, S. Pattathil, M. Li, W. Shen, C.A. Particka, S.D. Karlen, T. Phongpreecha, R.R. Semaan, E. Gonzales-Vigil, J. Ralph, S.D. Mansfield, S.-Y. Ding, D.B. Hodge, E.L. Hegg, Engineered Lignin in Poplar Biomass Facilitates Cu-Catalyzed Alkaline-Oxidative Pretreatment, ACS Sustainable Chemistry & Engineering 6(3) (2018) 2932-2941. https://doi.org/10.1021/acssuschemeng.7b02067.

[37] X. Zhang, T. Wang, L. Ma, Q. Zhang, X. Huang, Y. Yu, Production of cyclohexane from lignin degradation compounds over Ni/ZrO2–SiO2 catalysts, Applied Energy 112 (2013) 533-538.

https://doi.org/10.1016/j.apenergy.2013.04.077.

[38] H. Liu, L. Zhu, A.-M. Wallraf, C. Räuber, P.M. Grande, N. Anders, C. Gertler, B. Werner, J. Klankermayer, W. Leitner, U. Schwaneberg, Depolymerization of Laccase-Oxidized Lignin in Aqueous Alkaline Solution at 37 °C, ACS Sustainable Chemistry & Engineering 7(13) (2019) 11150-11156. https://doi.org/10.1021/acssuschemeng.9b00204.

[39] Q. Lu, L. Jia, M.K. Awasthi, G. Jing, Y. Wang, L. He, N. Zhao, Z. Chen, Z. Zhang, X. Shi, Variations in lignin monomer contents and stable hydrogen isotope ratios in methoxy groups during the biodegradation of garden biomass, Sci Rep 12(1) (2022) 8734. https://doi.org/10.1038/s41598-022-12689-1.

[40] K. Przybysz Buzała, H. Kalinowska, E. Małachowska, P. Przybysz, The utility of selected kraft hardwood and softwood pulps for fuel ethanol production, Industrial Crops and Products 108 (2017) 824-830. https://doi.org/10.1016/j.indcrop.2017.07.038.

[41] X. Xu, R. Pan, R. Chen, Comparative Thermal Degradation Behaviors and Kinetic Mechanisms of Typical Hardwood and Softwood in Oxygenous Atmosphere, Processes 9(9) (2021). https://doi.org/10.3390/pr9091598.

[42] Y. Ding, O.A. Ezekoye, S. Lu, C. Wang, R. Zhou, Comparative pyrolysis behaviors and reaction mechanisms of hardwood and softwood, Energy Conversion and Management 132 (2017) 102-109. https://doi.org/10.1016/j.enconman.2016.11.016.

[43] Y. Mottiar, S.D. Mansfield, Lignin p-Hydroxybenzoylation Is Negatively Correlated With Syringyl Units in Poplar, Frontiers in Plant Science 13 (2022). https://doi.org/10.3389/fpls.2022.938083.

[44] M. Eisenlauer, U. Teipel, Comminution energy and particulate properties of cutting and hammer-milled beech, oak, and spruce wood, Powder Technology 394 (2021) 685-704. https://doi.org/10.1016/j.powtec.2021.03.072.

[45] A. Martínez-Abad, N. Giummarella, M. Lawoko, F. Vilaplana, Differences in extractability under subcritical water reveal interconnected hemicellulose and lignin recalcitrance in birch hardwoods, Green Chemistry 20(11) (2018) 2534-2546. https://doi.org/10.1039/c8gc00385h.

[46] O.A. Levitskiy, V.V. Sentyurin, T.V. Magdesieva, Twisting of diarylnitroxides: An efficient tool for redox tuning, Electrochimica Acta 260 (2018) 459-467. https://doi.org/10.1016/j.electacta.2017.11.168.

[47] C. Cao, Z. Zeng, C. Cao, A new insight into the push-pull effect of substituents via the stilbene-like model compounds, Journal of Physical Organic Chemistry 35(4) (2022). https://doi.org/10.1002/poc.4319.

[48] Y.H. Liao, S.F. Koelewijn, G. Van den Bossche, J. Van Aelst, S. Van den Bosch, T. Renders, K. Navare, T. Nicolai, K. Van Aelst, M. Maesen, H. Matsushima, J.M. Thevelein, K. Van Acker, B. Lagrain, D. Verboekend, B.F. Sels, A sustainable wood biorefinery for low-carbon footprint chemicals production, SCIENCE 367(6484) (2020) 1385-+. https://doi.org/10.1126/science.aau1567.

[49] W.-D. Schneider, C. Laubschat, Actinide—noble-metal systems: An x-ray-photoelectron-spectroscopy study of thorium-platinum, uranium-platinum, and uranium-gold intermetallics, Physical Review B 23(3) (1981) 997-1005. https://doi.org/10.1103/PhysRevB.23.997.

[50] A.A. Siller-Ceniceros, M.E. Sánchez-Castro, D. Morales-Acosta, J.R. Torres-Lubian, E. Martínez G, F.J. Rodríguez-Varela, Innovative functionalization of Vulcan XC-72 with Ru organometallic complex: Significant enhancement in catalytic activity of Pt/C electrocatalyst for the methanol oxidation reaction (MOR), Applied Catalysis B: Environmental 209 (2017) 455-467. https://doi.org/10.1016/j.apcatb.2017.03.023.

[51] A. Ali, C. Zhao, Ru nanoparticles supported on hydrophilic mesoporous carbon catalyzed low-

temperature hydrodeoxygenation of microalgae oil to alkanes at aqueous-phase, Chinese Journal of Catalysis 41(8) (2020) 1174-1185. https://doi.org/10.1016/s1872-2067(20)63539-2.

[52] J. Zhang, X. Zhang, G. Xia, Y. Zhang, L. Di, Cold plasma for preparation of Pd/C catalysts toward formic acid dehydrogenation: Insight into plasma working gas, Journal of Catalysis 400 (2021) 338-346. https://doi.org/10.1016/j.jcat.2021.06.019.

[53] E. Kordouli, C. Kordulis, A. Lycourghiotis, R. Cole, P.T. Vasudevan, B. Pawelec, J.L.G. Fierro, HDO activity of carbon-supported Rh, Ni and Mo-Ni catalysts, Molecular Catalysis 441 (2017) 209-220. https://doi.org/10.1016/j.mcat.2017.08.013.

[54] W. Sun, S. Wu, Y. Lu, Y. Wang, Q. Cao, W. Fang, Effective Control of Particle Size and Electron Density of Pd/C and Sn-Pd/C Nanocatalysts for Vanillin Production via Base-Free Oxidation, ACS Catalysis 10(14) (2020) 7699-7709. https://doi.org/10.1021/acscatal.0c01849.

[55] N. Singh, Y. Song, O.Y. Gutiérrez, D.M. Camaioni, C.T. Campbell, J.A. Lercher, Electrocatalytic Hydrogenation of Phenol over Platinum and Rhodium: Unexpected Temperature Effects Resolved, ACS Catalysis 6(11) (2016) 7466-7470. https://doi.org/10.1021/acscatal.6b02296.

[56] Q. Zhai, S. Han, C.-Y. Hse, J. Jiang, J. Xu, Electrocatalytic hydrogenation of mono- and dimeric lignin to hydrocarbons in fluidized electrocatalytic system, Fuel Processing Technology 227 (2022). https://doi.org/10.1016/j.fuproc.2021.107109.

[57] H. Zhou, Z. Li, S.M. Xu, L. Lu, M. Xu, K. Ji, R. Ge, Y. Yan, L. Ma, X. Kong, L. Zheng, H. Duan, Selectively Upgrading Lignin Derivatives to Carboxylates through Electrochemical Oxidative C(OH)-C Bond Cleavage by a Mn-Doped Cobalt Oxyhydroxide Catalyst, Angew Chem Int Ed Engl 60(16) (2021) 8976-8982. https://doi.org/10.1002/anie.202015431.

[58] Y. Zhou, Y. Gao, X. Zhong, W. Jiang, Y. Liang, P. Niu, M. Li, G. Zhuang, X. Li, J. Wang, Electrocatalytic Upgrading of Lignin-Derived Bio-Oil Based on Surface-Engineered PtNiB Nanostructure, Advanced Functional Materials 29(10) (2019). https://doi.org/10.1002/adfm.201807651.

[59] K. Jiang, G. Bian, Y. Pan, G. Lai, Recognizing ortho-, meta- or para-positional isomers of S-methyl methoxylphenylmethylenehydrazine dithiocarboxylates by ESI-MS2: The positional effect of the methoxyl substituent, International Journal of Mass Spectrometry 299(1) (2011) 13-19. https://doi.org/10.1016/j.ijms.2010.09.004.